



Some physical properties of nanostructured Al doped ZnO thin films synthesized by RF magnetron sputtering at room temperature

Volkan Şenay¹

Published online: 12 April 2019

© Springer Science+Business Media, LLC, part of Springer Nature 2019

Abstract

In this research, AZO thin films were deposited on glass substrates with 70 W, 100 W and 125 W RF powers at room temperature by RF magnetron sputtering technique. The structural, optical and surface properties of the produced thin films were investigated. According to the obtained results, the investigated thin films had a crystalline structure and they showed high transparency in the visible region. The increase of RF power produced thicker films. Relatively thicker AZO films produced with higher RF power exhibited greater number of interference fringes in the reflectance and transmittance spectra. The refractive index values of the film produced with 125 W RF power were considerably lower than those of the films produced with 70 W and 100 W due to the decreased packing density. The optical energy band gap values of the produced AZO thin films were higher than that of undoped ZnO films. This expansion resulted from the Burstein–Moss effect. However, the band gap energy value as well as the roughness of the film surface decreased like refractive index with an increase in RF power, especially after 100 W. As a result, the values corresponding to the optical and surface properties can be tuned and AZO thin films can be produced by RF magnetron sputtering technique as promising candidates for optoelectronic devices and transparent conductive oxide applications.

1 Introduction

Transparent conducting oxides (TCOs) are unique types of materials combining optical transparency and electrical conductivity [1, 2]. Recently, TCO thin films have been widely adopted in the production of electronic and optoelectronic devices such as flat panel displays, LCDs, touch screens, blue or ultra-violet LEDs, gas sensors, laser diodes, organic LEDs, chemical sensors, thin-film transistors, and thin-film solar cells [3–8]. The performances of these devices depend on the electrical and optical properties of the TCO materials. Among the known TCO materials, tin-doped indium oxide (ITO) is the most favorable due to its electrical and optical properties [9–11]. However, ITO use is limited because of its scarcity, high price and toxicity [12, 13]. Due to the growing demand for high performance and low cost TCO films, it is necessary to investigate how superior electrical and optical characteristics of such films can be obtained economically [14]. In this context, undoped and doped zinc oxide

thin films are considered as promising candidates for TCO applications [15–17]. Especially, aluminum-doped ZnO (AZO) has attracted much attention as a replacement for ITO because of desirable properties such as long-term environmental stability, high optical transmittance in the visible region, wide band gap (from 3.4 to 3.9 eV), high electrical conductivity, non-toxicity, abundance and low cost [18–22]. AZO films show higher level of optical transparency when compared to undoped ZnO. Additionally, they exhibit lower electrical resistivity and better stability. Although AZO thin films possess these advantages, their electrical and optical properties are not better than those of ITO films. Therefore, how to deposit a high quality AZO film becomes an important issue in the TCO applications [23]. The motivation of the current research is to manufacture good quality AZO thin films as an alternative of ITO thin films for the existing TCO applications.

The physical properties of AZO thin films are generally dependent on deposition techniques and conditions [24]. To produce AZO thin films on different substrates, several deposition techniques have been used such as radio frequency (RF) or direct current (DC) magnetron sputtering [25, 26], molecular beam epitaxy (MBE) [27], metal–organic chemical vapor deposition (MOCVD) [28], sol–gel [29], spray

✉ Volkan Şenay
vsenay@bayburt.edu.tr

¹ Department of Opticianry, Bayburt University,
69000 Bayburt, Turkey

pyrolysis [30], and pulsed laser deposition (PLD) [31]. Every deposition method has its advantages and disadvantages in accordance with their usage [32]. Among these techniques, magnetron sputtering is the most common one utilized for depositing AZO thin films due to its repeatability, low cost, parameter controllability, high deposition rate, low processing temperature, good adhesion of films on substrates, good thickness uniformity and high stability for large-area films [33]. By optimizing deposition parameters (e.g. sputtering power, pressure and target-substrate distance), high quality films can be obtained. Numerous studies reveal that the AZO thin films with good crystalline structure show better electrical and optical properties than those with amorphous structures [34, 35]. Achieving good crystalline structure at a relatively low process temperature is the key to prepare highly conductive and transparent AZO thin films [36]. The related previous researches also argue that the layer thickness of the AZO films could have great influence on their properties [37–41]. In this work, AZO thin films having different thickness values are prepared on glass substrates at room temperature with different RF powers by RF magnetron sputtering. The effects RF power and film thickness on the optical and surface properties of AZO thin films are examined.

2 Experimental details

In the current research, the AZO thin films were deposited on 75 mm × 25 mm × 1 mm glass substrates in three separate experiments with 70 W, 100 W and 125 W RF powers by RF magnetron sputtering technique at room temperature. A commercially available AZO target (99.99% purity) was used as source material for all deposition processes. The diameter and thickness of the target was 50 mm and 3 mm, respectively. The sputter gun was connected to an RF plasma source with a frequency of 13.56 MHz. Prior to each deposition, the substrate was ultrasonically cleaned to ensure strong adhesion between the substrate and the AZO layer. After cleaning, the substrate was directly fixed on a substrate holder positioned at 40 mm away from the target in all cases. For all depositions, sputtering chamber was evacuated down to 10^{-3} Torr by a mechanical pump and then filled with high-purity (99.99%) Ar gas. Chamber pressure was sustained to be 8×10^{-2} Torr. Each deposition process was carried out for 45 min. Only top surfaces of the substrates were coated with AZO. Deposition parameters are summarized in Table 1. The AZO thin films deposited at the RF powers of 70, 100, and 125 W are labeled as AZO70, AZO100 and AZO125, respectively.

The produced AZO thin films were investigated by several instrumentation techniques. The crystalline structure was examined in the 2θ range of 30° – 90° by using an X-ray

Table 1 Sputtering parameters of AZO thin films

RF power (W)	Substrate to target distance (mm)	Working pressure (Torr)	Time (min)
70, 100, 125	40	8×10^{-2}	45

diffractometer (PANalytical Empyrean) with monochromated $\text{CuK}\alpha$ radiation ($\lambda = 1.54056 \text{ \AA}$). The reflectance data were collected in the wavelength range of 400–1000 nm by an interferometer (Filmetrics F20 Thin Film Analyzer). The film thickness (t) and spectral distribution of refractive index (n) were obtained through the spectral analysis of reflectance. The optical transmittance and absorbance spectra were recorded at normal incidence of light with a double beam UV–Vis spectrophotometer (UNICO 4802). The spectral region observed was 300–1100 nm. The optical energy band gap values were then derived from the obtained absorbance data according to Tauc's method. In order to illustrate the surface topography, the two dimensional and three dimensional images were taken over a scale of $4 \mu\text{m} \times 4 \mu\text{m}$ in non-contact mode by using an AFM (Ambios Q-Scope).

3 Results and discussion

Figure 1 shows the X-ray diffraction patterns of the produced AZO thin films. The strong peaks show the crystalline nature of the films. A series of ZnO characteristic planes ($2\theta = 31.55^\circ$ (100), 34.13° (002), 36.18° (101), 72.26° (004) and 89.12° (203)) are observed. According to JCPDS (36-1451) and relevant literature [42, 43], these planes belong to hexagonal wurtzite phase of ZnO. The other peaks observed at 2θ values of 41.88° and 44.55° correspond to the (006) and (400) diffraction planes of hexagonal Al_2O_3 (JCPDS card no. 71-1123) and cubic spinel structure of ZnAl_2O_4 (JCPDS card no. 74-1138) in accordance with relevant literature [44, 45], respectively. No phases corresponding to elemental Al or Zn were detected in any of the samples.

The reflectance spectra of the produced AZO films are presented in Fig. 2. Multiple reflections between the front and back interfaces of the films coherently interfere with one another and the reflectance spectra exhibit interference fringe patterns. The amplitude and periodicity of the reflectance are determined by the film's thickness and optical constants. By using this phenomenon, the thickness values obtained by interferometer are 150 nm, 295 nm and 420 nm for the films produced with 70 W, 100 W and 125 W, respectively. According to these findings, it is found that relatively thicker AZO films exhibit greater number of oscillations over the observed wavelength range while thinner AZO films exhibit lesser number of oscillations or only part of an oscillation over the same range.

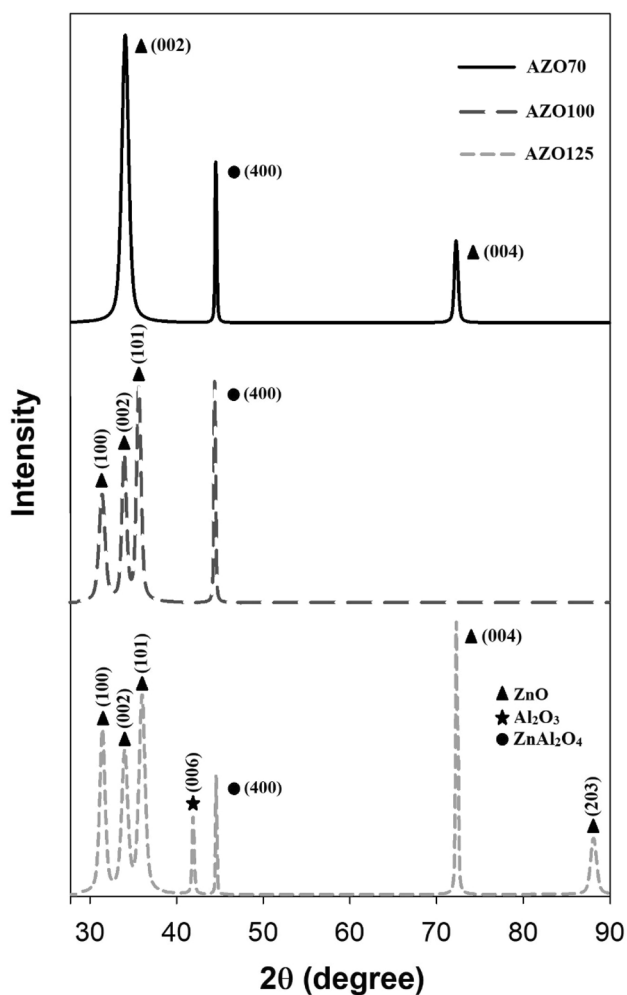


Fig. 1 XRD patterns of the produced AZO thin films

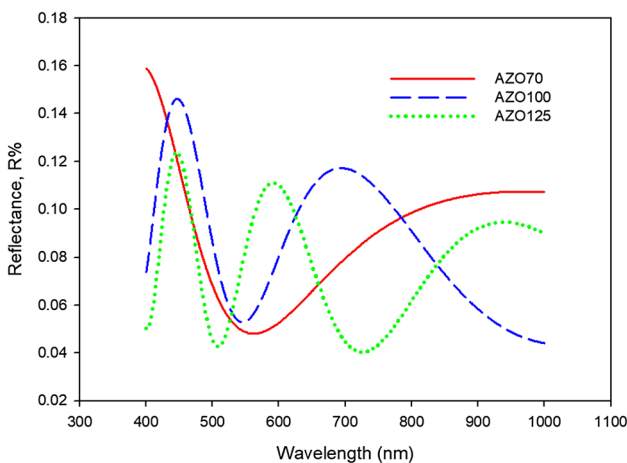


Fig. 2 Reflectance spectra of the produced AZO thin films

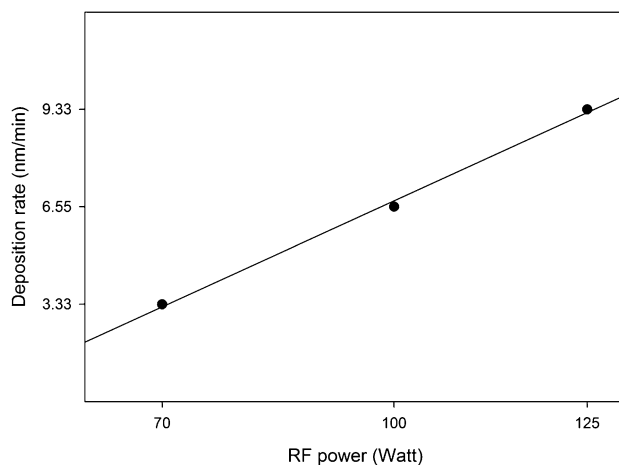


Fig. 3 Deposition rates of the produced AZO thin films versus RF power applied to the target

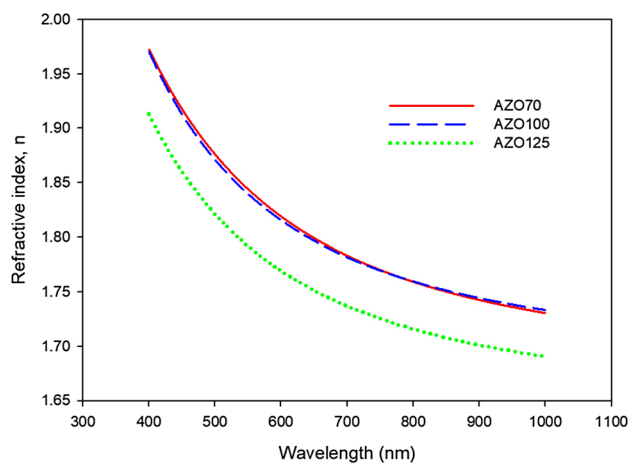


Fig. 4 Refractive index spectra of the produced AZO thin films

The deposition rates of the produced AZO thin films are calculated from the obtained film thickness values and the elapsed deposition time. The deposition rate is the film thickness divided by the deposition time. When the substrate to target distance and working pressure remain fixed in sputtering, the deposition rate is determined by the RF power. Figure 3 shows the deposition rate of the produced films as a function of the RF power. The figure shows that the deposition rate is heavily dependent on RF power. During the sputtering process, increased RF power produces more argon ions with higher kinetic energy in plasma. Therefore, the bombardment of argon ions on the target increases accordingly. As a result, the deposition rate increases with increasing sputtering power.

The refractive index distributions of the produced AZO thin films are represented in Fig. 4. Al doping reduces the refractive

indices of ZnO thin films due to an increase in the carrier concentration [46]. The decrease of refractive index value with increasing wavelength shows the normal dispersion behavior of the material. The distribution curves of the AZO thin films produced at 70 W and 100 W are almost identical. However, the refractive index values of the AZO film produced at 125 W RF power are considerably lower than those of the AZO films deposited at 70 W and 100 W which has been attributed to the decreased packing density of the film. A previous research in literature also indicates that the packing density tends to decrease with an increase in RF power, particularly showing a sudden decrease after 100 W [47].

The optical transmittance and absorbance spectra of the AZO films deposited with different RF powers are presented in Fig. 5. It is observed that the transmittance spectra coincide with the recorded reflectance spectra. The oscillatory character of the transmittance curves is due to the interference effect arising from the multiple reflections at the interfaces. The number of interference fringes increases as the film thickness increases. All of the produced AZO thin films exhibit an average transmittance rate above 80% in the visible region from 400 to 700 nm and a sharp fundamental absorption edge in the UV region. The absorption edge in the UV region has a red shift with the increasing RF power. Investigating the shape and shift of the absorption edge is a highly fruitful technique for revealing the basic mechanism of optically induced transitions as the absorption edge is related to the optical band gap energy.

The optical absorption coefficients (α) or the produced AZO thin films are calculated using the following expression [48]:

$$\alpha = 2.303(A/t) \tag{1}$$

where t is the film thickness and A is the optical absorbance. Further, the relationship between absorption coefficient (α) and incident photon energy ($h\nu$) can be expressed as [49]:

$$ah\nu = B(h\nu - E_g)^n \tag{2}$$

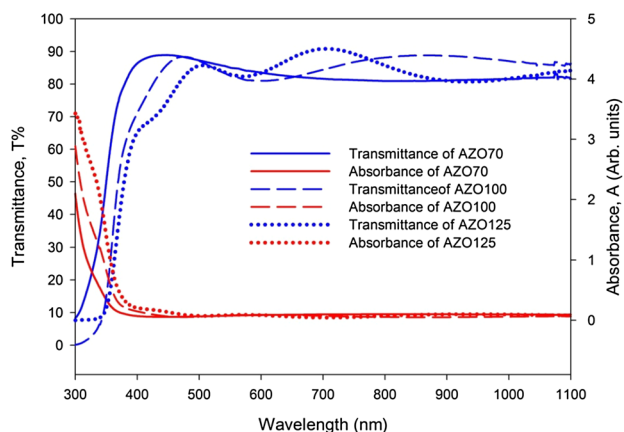


Fig. 5 Optical transmittance and absorbance spectra of the produced AZO thin films

where B is energy independent constant, E_g is optical energy band gap of the material and the exponent n depends on the type of transition. The n value takes 2 and 1/2 for allowed indirect and allowed direct transitions, respectively. Figure 6 shows the plot of $(ah\nu)^2$ versus $h\nu$. The single slope in the figure asserts that the produced AZO films have direct and allowed transition. The band gap energy is obtained by extrapolating the straight line portion of the plot to zero absorption coefficient. The band gap values are found to be 3.62 eV, 3.56 eV and 3.46 eV for the films produced with the RF powers of 70 W, 100 W and 125 W, respectively. Thus, the energy band gap decreases due to the increase in the film thickness, in accordance with previous literature data [50]. When compared to the undoped ZnO thin films, higher band gap values of the produced AZO thin films can be attributed to the well-known Burstein Moss effect which is a result of increased free electron concentration with Al doping. Fermi energy level increases with the increasing electron concentration which causes the widening of the band gap. Since the increasing sputtering power caused a decrease of carrier concentration, the widening of the optical band gap was moderated, and the optical band gap energy values of AZO thin films decreased in a previous related research [51]. The desirable energy band gap value of TCOs is a wide one above 3.2 eV. Such a value allows most light from the solar spectrum to pass through the TCO films instead of being absorbed.

The two dimensional (2D) and three dimensional (3D) AFM images of the produced AZO thin films are presented in Fig. 7. The surface images of the AZO film deposited at 70 W show some valleys and hillocks. When the RF power is increased to 100 W, valleys are found to increase while hillocks decrease. In the case of 125 W, the number of valleys decreases and hillocks increase due to the formation of regular shaped smaller grains. Surface roughness is one of the most significant characteristics of the AZO thin films

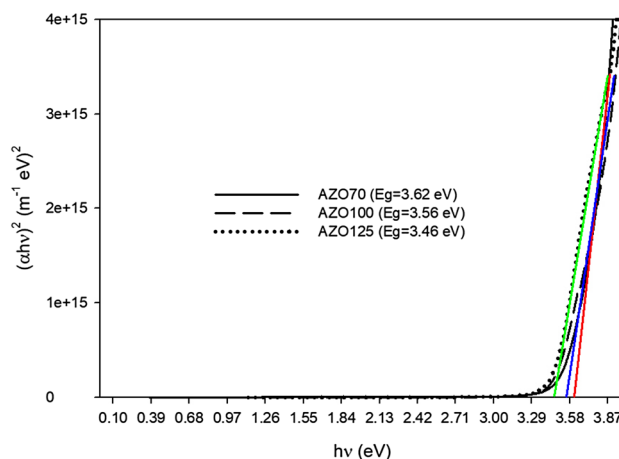


Fig. 6 Tauc plot of $(ah\nu)^2$ versus $h\nu$

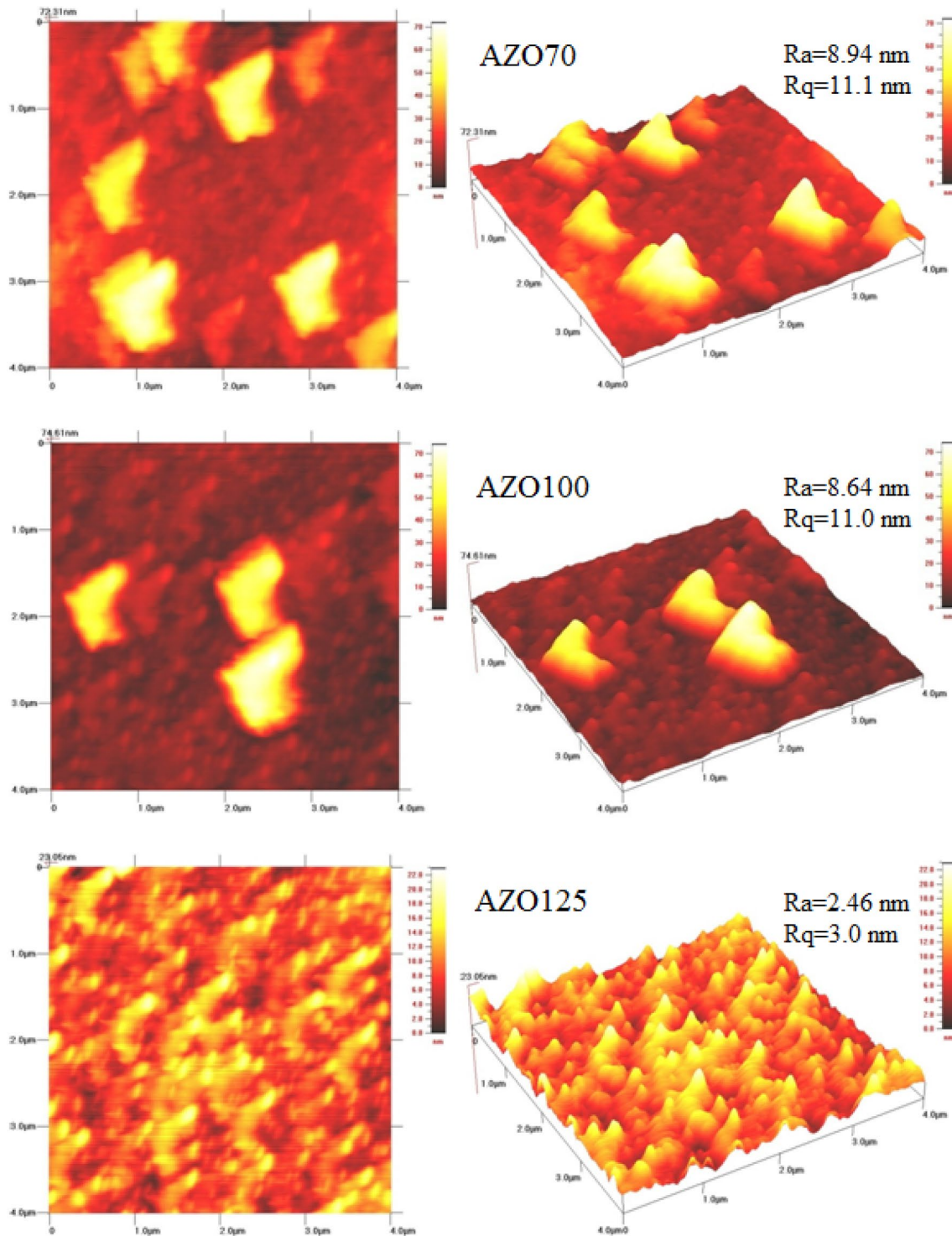


Fig. 7 2D and 3D AFM images of the produced AZO thin films

for many opto-electronic applications, because the level of surface roughness affects the carrier mobility and light scattering. An AZO thin film with a surface roughness of $\sim 10 \text{ nm}$ is sufficient to meet the requirements for optical device applications [3]. The average surface roughness (R_a)

values of the produced AZO thin films vary between 2.46 and 8.94 nm. Root mean square roughness (R_q) values are 11.1, 11.0 and 3.0 nm for the films deposited with 70 W, 100 W and 125 W, respectively. As a result, the increase of RF power produces AZO thin films with higher degree of

surface uniformity while the roughness value decreases with the increasing RF power, especially after 100 W. Stability of semiconductor devices heavily depend on TCO/semiconductor interface quality. A non-uniform surface can bring about breakdown or shortening with upper layers. This may cause severe complexities on the performance of electrical and optical devices.

4 Conclusion

In conclusion, monolayer AZO thin films having ;crystal-line structure and high level of transparency (above 80% in the visible region) were deposited on glass substrates at room temperature with different RF powers by RF magnetron sputtering. The deposition rate, as well as film thickness increases with the increasing RF power. Relatively thicker AZO films produced with higher RF power exhibit greater number of oscillations in reflectance and transmittance spectra. The refractive index values of the film produced at 125 W RF power are considerably lower than those the films deposited at 70 W and 100 W in accordance with literature. The absorption edge in the UV region has a red shift with the increasing RF power. Thus, the energy band gap decreases as a result of the increase in RF power and/or film thickness value. The surface morphology of a produced thin film is related to the mobility of the deposited atoms at the growing film surface and depends on the processing parameters such as RF power in sputtering. This study shows that relatively higher RF power such as 125 W is suitable for obtaining AZO thin films with good surface characteristics.

References

1. M. Fallah, M.-R. Zamani-Meymian, R. Rahimi, M. Rabbani, Appl. Surf. Sci. **316**, 456 (2014)
2. T. Gu, E.-T. Hu, S. Guo, et al., Vacuum **163**, 69 (2019)
3. D.K. Kima, H.B. Kimb, Appl. Sci. Converg. Technol. **23**, 279 (2014)
4. C. Guillén, J. Herrero, Thin Solid Films **520**, 1 (2011)
5. M.-C. Jun, S.-U. Park, J.-H. Koh, Nanoscale Res. Lett. **7**, 1 (2012)
6. A.A. Al-ghamdi, H. Alhumminay, M.S. Abdel-wahab, I. Yahia, Optik-Int. J. Light Electron Opt. **127**(10), 4324–4328 (2016)
7. T. Yang, S. Song, Y. Li et al., Physica B **407**, 4518 (2012)
8. C. Ma, X. Lu, B. Xu, et al., J. Alloys Compd. **774**, 201 (2018)
9. T.-C. Lin, W.-C. Huang, F.-C. Tsai, Thin Solid Films **589**, 446 (2015)
10. Y.S. Jung, Y.S. Park, K.H. Kim, W.-J. Lee, Trans. Electr. Electr. Mater. **14**, 9 (2013)
11. W. Zhang, J. Gan, L. Li et al., Mater. Sci. Semicond. Process. **74**, 147 (2018)
12. A. Eshaghi, M. Hajkarimi, Optik-Int. J. Light Electron Opt. **125**, 5746 (2014)
13. P.-C. Yao, S.-T. Hang, M.-J. Wu, Trans. Can. Soc. Mech. Eng. **37**, 303–312 (2013)
14. C.-H. Chu, H.-W. Wu, J.-L. Huang, Ceram. Int. **42**(5), 5754–5761 (2016)
15. B. Efafi, M.S. Ghamsari, M.M. Ara, J. Lumin. **154**, 32 (2014)
16. Y.-S. Liu, C.-Y. Hsieh, Y.-J. Wu et al., Appl. Surf. Sci. **282**, 32 (2013)
17. J. Li, X. Zhu, Q. Xie, D. Yang, Ceram. Int. **45**, 3871 (2019)
18. J. Chen, Y. Sun, X. Lv et al., Appl. Surf. Sci. **317**, 1000 (2014)
19. P. Prepelita, V. Craciun, F. Garoi, A. Staicu, Appl. Surf. Sci. **352**, 23 (2015)
20. H. Wu, C. Chu, Y. Chen, et al., in *Proceedings of the International MultiConference of Engineers and Computer Scientists (IMECS)*, HongKong, 13–15 March 2013, vol. **II** (2013)
21. K. Sun, X. Tang, C. Yang, D. Jin, Ceram. Int. **44**, 19597 (2018)
22. A. Landa-Cánovas, J. Santiso, F. Agulló-Rueda et al., Ceram. Int. **45**, 6319 (2019)
23. R. Chang, T. Li, C. Lin, Appl. Surf. Sci. **258**, 3732 (2012)
24. H. Park, S.Q. Hussain, S. Velumani et al., Mater. Sci. Semicond. Proc. **37**, 29 (2015)
25. A. Spadoni, M. Addonizio, Thin Solid Films **589**, 514 (2015)
26. A. Barhoumi, G. Leroy, B. Duponchel et al., Superlattices Microstruct. **82**, 483 (2015)
27. T. Ohgaki, Y. Kawamura, T. Kuroda, et al., Key Eng. Mater. Trans Tech. Publ. **248**, 91 (2003)
28. M.E. Fragala, G. Malandrino, M.M. Giangregorio et al., Chem. Vap. Depos. **15**, 327 (2009)
29. M. Ohyama, H. Kozuka, T. Yoko, J. Am. Ceram. Soc. **81**, 1622 (1998)
30. A. Aktaruzzaman, G. Sharma, L. Malhotra, Thin Solid Films **198**, 67 (1991)
31. C. Weigand, R. Crisp, C. Ladam et al., Thin Solid Films **545**, 124 (2013)
32. A. Jilani, M.S. Abdel-wahab, A.A. Al-ghamdi, A. Sadik Dahlan, I. Yahia, Physica B **481**, 97 (2016)
33. M. Naddaf, M. Saad, Vacuum **122**, 36 (2015)
34. C. Guillen, J. Herrero, Vacuum **84**, 924 (2010)
35. J. Chang, H.-L. Wang, M.-H. Hon, J. Cryst. Growth **211**, 93 (2000)
36. L. Wen, B.B. Sahu, H.R. Kim, J.G. Han, Appl. Surf. Sci. **473**, 649 (2019)
37. K.H. Ri, Y. Wang, W.L. Zhou, J.X. Gao, X.J. Wang, J. Yu, Appl. Surf. Sci. **258**, 1283 (2011)
38. K.-W. Seo, H.-S. Shin, J.-H. Lee, K.-B. Chung, H.-K. Kim, Vacuum **101**, 250 (2014)
39. F. Garcés, N. Budini, R. Arce, J. Schmidt, Thin Solid Films **574**, 162 (2015)
40. S. Rahmane, M.S. Aida, M.A. Djouadi, N. Barreau, Superlattices Microstruct. **79**, 148 (2015)
41. F. Wang, M. Wu, Y. Wang, Y. Yu, X. Wu, L. Zhuge, Vacuum **89**, 127 (2013)
42. W.-C. Huang, J.L. Chiu, X.D. Lin et al., Results Phys. **10**, 132 (2018)
43. J. Suresh, G. Pradheesh, V. Alexramani, M. Sundrarajan, S.I. Hong, Adv. Nat. Sci.: Nanosci. Nanotechnol. **9**, 015008 (2018)
44. S. Kumar, V. Mote, R. Prakash, V. Kumar, Mater. Focus **5**, 545 (2016)
45. X. Yong, F. Ping, Z. Baohua, G. Juan, Z. Lin, W. Xuehua, Mater. Lett. **123**, 142 (2014)
46. Q.H. Li, D. Zhu, W. Liu, Y. Liu, X.C. Ma, Appl. Surf. Sci. **254**, 2922 (2008)
47. B.C. Mohanty, D.H. Yeon, J.H. Yun, J.S. Cho, Y.S. Cho, Appl. Phys. A **115**, 347 (2014)
48. V. Şenay, S. Özen, S. Pat, Ş. Korkmaz, Mater. Focus **4**, 397 (2015)
49. J. Tauc, R. Grigorov, A. Vancu, Phys. Status Solidi **15**, 627 (1966)
50. N. Srinatha, Y. No, V.B. Kamble et al., RSC Adv. **6**, 9779 (2016)
51. Y.-H. Sun, C. H-l Wang, F.Liang Jian, W. Lei, Trans. Nonferrous Met. Soc. China **26**, 1655 (2016)

Publisher's Note Springer Nature remains neutral with regard to jurisdictional claims in published maps and institutional affiliations.